Available online at www.sciencedirect.com
SCIENCE DIRECT
Polymer 47 (2006) 883–896
polymer
www.elsevier.com/locate/polymer

A QM/MM study of the ethylene and styrene insertion process into the ion pair $[Me_2Si(C_5Me_4)(N^tBu)Ti(CH_2CH_2CH_3)]^+[\mu\text{-}Me\text{–}Al(Me)_2\text{–}(AlOMe)_6Me]^-$

S. Martínez, J. Ramos, V.L. Cruz *, J. Martínez-Salazar

Departamento de Física Macromolecular, Instituto de Estructura de la materia, CSIC, Serrano 113bis, 28006 Madrid, Spain

Received 28 September 2005; accepted 5 December 2005

Abstract

Ethylene and styrene insertion into the metal–alkyl bond of $[Me_2Si(C_5Me_4)(N^tBu)Ti\ (CH_2CH_2CH_3)]^+[\mu\text{-}Me\text{–}Al(Me)_2\text{–}(AlOMe)_6Me]^-$ species has been investigated using a QM/MM approach. Validation of the B3LYP//B3LYP/UFF theoretical model was performed by comparing some results with full QM calculations. Ion pairs which contain a bounded trimethylaluminium molecule give rise to active species, whereas direct coordination of the MAO cage to the catalyst leads to dormant species for polymerisation. Ion pair formation and dissociation for both ion-pair complexes have been performed. In addition, monomer insertions into the active ion-pair species have been studied. The monomer coordination step results to be endothermic in contrast to the values obtained for the 'naked' cation. The energetic insertion barriers starting from the π-complexes are similar to those obtained for the 'naked' cationic species. The net effect of the cocatalyst is to increase the coordination barriers at a similar amount for two-monomer insertions. Some implications of the cocatalyst effect in ethylene/styrene copolymerisation are discussed.

Keywords: Geometry constrained catalyst; Methylaluminoxane cocatalyst; Ethylene–styrene insertion

1. Introduction

The interest in metallocene catalysts for olefin polymerisation is continuously growing due to its high selectivity and activity. The presence of a cocatalyst is essential for the polymerisation process to take place. Experimental evidences exist indicating the influence of both cocatalyst and solvent in the catalyst activity and selectivity [1,2]. Methylaluminoxane (MAO) is one of the most commonly used cocatalyst because it has shown to be highly active. However, the existence of multiple equilibriums between different $(AlOMe)_n$ oligomers makes very difficult the complete MAO structure determination. Several theoretical works have been published in the literature to seed light about the structural behaviour of the MAO compound. These works can be divided in two main blocks: on one side, those studies dealing with the pure MAO structure and on the other hand those regarding the interaction of MAO with trimethylaluminium (TMA), a situation which is more real.

The 'pure' MAO structure seems to have preference for cage geometries with four and six member sides, as it has been concluded by several theoretical [3–5] and experimental [6] studies. This disposition allows the existence of 'latent' acidic aluminium centres as a consequence of the ring strain present in the MAO cages. These centres are able to extract a methyl group of the dialkyl catalytic precursor, forming the ion-pair complexes between the catalyst precursor and the cocatalyst species.

The interaction between 'pure' MAO and TMA constitutes the so-called 'real' MAO system, which is actually present in the reaction media. The structure of the 'real' MAO has been theoretically studied by several authors [3,7–9] pointing out that MAO cages with a number of $[MeAlO]_n$ units between 6 and 12 are able to interact with TMA molecules forming stable compounds. The general mechanism of this reaction contemplates the rupture of a square side by breaking an Al–O bond. A methyl group belonging to the TMA molecule bonds to the Al centre, whereas the remaining $AlMe_2$ group bonds the O atom.

The interaction between these MAO structures and the catalyst has been considered by only very few theoretical works in spite that MAO is the most used cocatalyst in experiments of this polymerisation type. From the early papers

* Corresponding author. Tel.: +34 915 616 800.
E-mail address: victor.cruz@iem.cfmac.csic.es (V.L. Cruz).

0032-3861/$ - see front matter © 2005 Elsevier Ltd. All rights reserved.
doi:10.1016/j.polymer.2005.12.013

of Fusco et al. [10,11] to the most recent paper of Belelli et al. [12], all the authors have shown the high energetic cost of the ion pair dissociation, even for the different models of the MAO structure considered in each work. Among these works, Ziegler's group published a series of papers considering different aspects of the catalyst/MAO interaction. The solvent effect on the ion pair separation process [13] showed that the enthalpy of ion pair separation (ΔH_{ips}) is halved when polar solvents are considered. The same work also considered the case of a toluene solvent molecule separating the two counterions, obtaining further stability over the ion pair separation reaction. However, the large volume of the catalyst ligands and the high olefin concentration in the reaction vessel might favour ethylene instead of toluene coordination [14].

In a later work, two different models for the ion pair have been proposed [15]: with and without bounded TMA to the MAO cage, which were in agreement with NMR experiments [16]. The compound without TMA presented a strong Zr–O interaction that produces a dormant catalyst system. The complex containing TMA gave rise to an active species due to the interposition of the alkylaluminium molecule in between the precursor catalyst and the MAO cage, which makes the ion pair separation more feasible. Later on, enthalpies of ion pair formation (ΔH_{ipf}) and separation (ΔH_{ips}) for these two species were evaluated with a series of different metallocene catalysts [17]. It was observed in general that the higher the $-\Delta H_{ipf}$ value the lower the calculated ΔH_{ips}. It was also concluded that bulky ligands tend to destabilize the ion pair due to the increase in steric hindrance between cation and anion.

These theoretical works suggest that ion pair dissociation prior to olefin complexation and insertion is an unlike event. However, very few papers consider the presence of cocatalyst in the theoretical study of the polymerisation process. The first one published by Bernardi et al. [18] obtained similar insertion barriers for ethylene in the 'naked' cation Cl_2TiMe^+ and in the $H_2Al(\mu\text{-}Cl)_2TiCl_2Me$ ion pair, for which an additional monomer complexation barrier was found. The Ziegler group also concluded that the rate determining step in the ethylene insertion into $[Cp_2ZrEt]^+$–$[MeB(C_6F_5)_3]^-$ was the monomer complexation [19]. The work of Lanza et al. [20] on the ethylene insertion into ionic $[H_2Si(C_5H_4)(N^tBu)Ti(n\text{-}C_3H_7)]^+[MeB(C_6F_5)_3]^-$ showed that the main effect of the anion was to increase the overall energy of the total insertion process. The complexation step was endothermic, but the energy barrier for the monomer insertion phase is very similar to that found for the 'naked' cationic species. To our best knowledge, the only paper found, where monomer insertion is contemplated in presence of MAO as cocatalyst was published by Zurek and Ziegler [21]. They proposed two mechanisms for olefin insertion into the Cp_2ZrMe_2 catalyst, dissociative and associative. These mechanisms differ mainly in the structure of the transition state, which is characterized by separation of the counterions in the former case and by a methyl bridge elongation in the associative one. Furthermore, the ethylene approximation can be cis or trans with respect to the methyl bridge, giving rise to different possibilities for the olefin insertion reaction.

With all this information into account we decided to tackle the study of the effect produced by the presence of cocatalyst in the ethylene/styrene copolymerisation process. Our group has published several papers regarding ethylene/styrene copolymerisation with different 'naked' catalyst systems [22–26]. In this work, we present the theoretical results obtained for the insertion of ethylene and 1,2-styrene in the constrained geometry catalysts $[Me_2Si(C_5Me_4)(N^tBu)TiMe_2]$ in the presence of MAO and TMA as cocatalyst. This Ti-based compound has been selected because it is one of the most commonly used catalyst in ethylene/styrene copolymerisation. The $(AlOMe)_6$ cage has been chosen for the MAO model in agreement with the considerations given above. The ion pair formation and dissociation processes have been investigated as a previous step to the study of the insertion reactions.

2. Computational methods

A Quantum Mechanics–Molecular Mechanics (QM/MM) approach based on the ONIOM scheme was selected due to the large size of the system [27]. For the QM part, the B3LYP hybrid DFT model was chosen [28,29]. The atoms in the Ti centre, the methyl bridge, the growing alkyl chain, both TMA methyl groups and the TMA aluminium were described by a DZVP

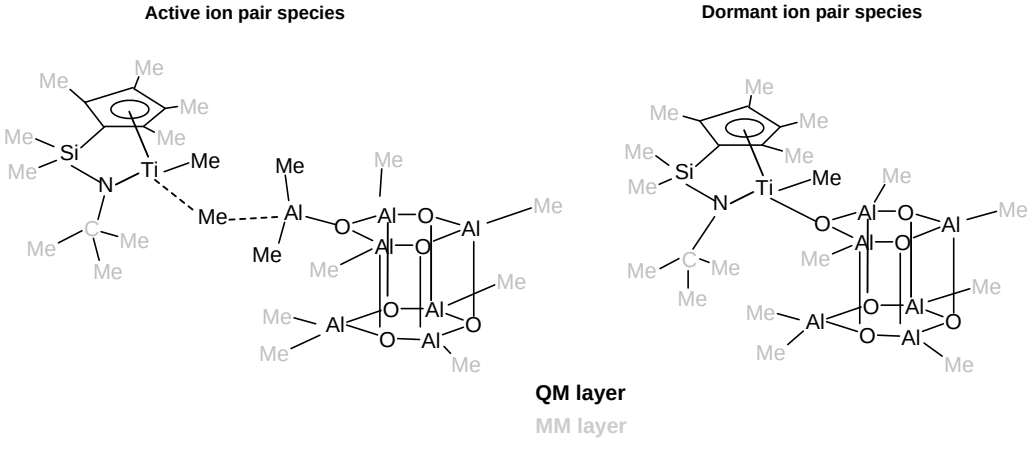

Scheme 1.

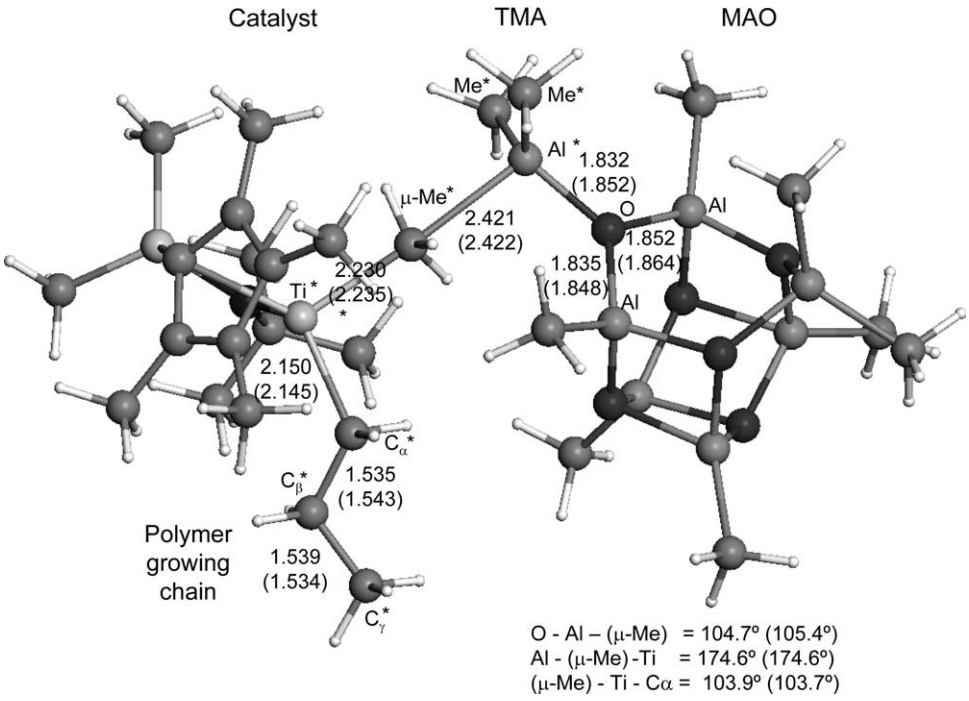

Fig. 1. Main geometric parameters of the active $[Me_2Si(C_5Me_4)(N^tBu)TiCH_2CH_2CH_3]^+[\mu\text{-Me–Al(Me)}_2\text{–(AOMe)}_6Me]^-$ ion-pair species calculated using the full DFT B3LYP method with two different basis sets DZVP/LANL2DZ and DZVP (given in the parentheses), respectively. For the DZVP/LANL2DZ optimisation, atoms with * are described in DZVP while the other atoms are described in LANL2DZ. Distances are given in angstrom and angles in degree.

Table 1
Geometric parameters for the ion-pair $[Me_2Si(C_5Me_4)(N^tBu)TiCH_2CH_2CH_3]^+[\mu\text{-Me–Al(Me)}_2\text{–(AOMe)}_6Me]^-$ species in QM/MM methods. Disturbances are given in angstroms and angles in degrees

Run	1	2	3	4	5	6
QM/MM atoms						
$C–C_{Cp}$	1.507–1.512	1.508	1.500	1.502	1.505	1.516
Si–C	1.897	1.880	1.882	1.884	1.886	1.903
N–C	1.506	1.462	1.463	1.462	1.463	1.471
Al–C	1.954–1.967	1.980–1.988	1.977–1.983	1.975–1.982	1.977–1.979	1.961–1.968
Al_{tetra}–C	1.986–1.996	2.004	2.002	2.000	1.998	1.990
C–Al–C	121.7	118.0	118.0	120.6	118.0	117.8
C–Si–C	106.0	109.5	109.0	109.2	109.1	109.3
QM atoms						
Ti–(μ-Me)	2.230	2.206	2.204	2.204	2.204	2.206
Al–(μ-Me)	2.421	2.524	2.520	2.524	2.536	2.509
Al–O	1.832	1.839	1.838	1.838	1.839	1.843
Ti–Cα	2.150	2.153	2.148	2.148	2.148	2.148
$Al–C_{TMA}$	1.974–1.975	1.974–1.975	1.974–1.976	1.975–1.976	1.974–1.976	1.974–1.975
Ti–N	1.947	1.963	1.965	1.966	1.965	1.964
C_{Cp}–C_{Cp}	1.436–1.455	1.430–1.457	1.433–1.457	1.434–1.457	1.433–1.456	1.432–1.456
$Al_{squared}$–O	1.852–1.952	1.859–1.967	1.859–1.969	1.859–1.968	1.859–1.968	1.860–1.968
Al_{hexag}–O	1.835–1.852	1.828–1.853	1.828–1.852	1.828–1.853	1.828–1.852	1.828–1.852
Al_{tetra}–O	1.874–1.879	1.873–1.876	1.873–1.876	1.873–1.875	1.873–1.875	1.870–1.873
Ti–Me–Al	174.6	171.7	171.9	171.7	171.7	171.8
Me–Al–O	104.7	100.3	99.6	99.4	99.4	99.5
Me–Ti–Cα	103.9	101.7	102.8	102.8	102.8	102.9
Ti–Cα–Cβ–Cγ	−82.3	−81.9	−82.9	−83.2	−83.2	−83.4
MM atoms						
C–C(*tert*)	1.549–1.554	1.534–1.544	1.533–1.544	1.534–1.539	1.533–1.544	1.539–1.544

Alpha values for each run (details in computational methods section): Run 1, full QM optimisation B3LYP/DZVP-LANL2DZ (details in section 2). Run 2, QM/MM optimisation: $\alpha_{Car}=0.724$; $\alpha_{Si}=0.781$; $\alpha_N=0.700$; $\alpha_{Al}=0.793$ (default parameters in Gaussian 03). Run 3, QM/MM optimisation: $\alpha_{Car}=0.719$; $\alpha_{Si}=0.776$; $\alpha_N=0.695$; $\alpha_{Al}=0.798$. Run 4, QM/MM optimisation: $\alpha_{Car}=0.714$; $\alpha_{Si}=0.771$; $\alpha_N=0.690$; $\alpha_{Al}=0.803$. Run 5, QM/MM optimisation: $\alpha_{Car}=0.709$; $\alpha_{Si}=0.766$; $\alpha_N=0.685$; $\alpha_{Al}=0.808$. Run 6, QM/MM optimisation: $\alpha_{Car}=0.674$; $\alpha_{Si}=0.731$; $\alpha_N=0.650$; $\alpha_{Al}=0.843$.

Table 2
Geometric parameters for the active ion-pair $[Me_2Si(C_5Me_4)(N^tBu)Ti(R)]^+[\mu\text{-Me–Al(Me)}_2\text{–(AOMe)}_6Me]^-$ species, where R = $CH_2CH_2CH_3$, $CH_2CH(Ph)CH_3$, $CH(Ph)CH_2CH_3$. Disturbances are given in angstroms.

R	Method	Ti–(μ-Me)	Ti–Cα	Al–(μ-Me)	Al–C_{TMA}	Al–O
$CH_2CH_2CH_3$	Full QM[a]	2.230	2.150	2.421	1.974–1.975	1.832
	QM/MM[b]	2.206	2.153	2.524	1.974–1.975	1.839
$CH_2CH(Ph)CH_3$	Full QM[a]	2.229	2.107	2.397	1.980–1.986	1.831
	QM/MM[b]	2.187	2.109	2.524	1.975–1.975	1.839
$CH(Ph)CH_2CH_3$	Full QM[a]	2.243	2.191	2.525	1.979–1.983	1.830
	QM/MM[b]	2.187	2.227	2.589	1.971–1.977	1.839

[a] B3LYP/DZVP-LANL2DZ method.
[b] QM/MM optimisation. QM layer: B3LYP/DZVP-LANL2DZ. MM layer: UFF force field. $\alpha_{Car}=0.724$; $\alpha_{Si}=0.781$; $\alpha_N=0.700$; $\alpha_{Al}=0.793$ (default parameters in Gaussian 03).

Table 3
Energy values in kcal/mol for the formation of active ion-pair $[Me_2Si(C_5Me_4)(N^tBu)Ti(R)]^+[\mu\text{-Me–Al(Me)}_2\text{–(AOMe)}_6Me]^-$ species, where R = CH_2CH_2 CH_3, $CH_2CH(Ph)CH_3$, $CH(Ph)CH_2CH_3$

R	ΔE_{QM}[a]	$\Delta E_{QM/MM}$[b]	$\Delta E_{QM//QM/MM}$[c]
$CH_2CH_2CH_3$	−6.0	−17.1	−6.8
$CH_2C(Ph)HCH_3$	−5.9	−13.9	−4.9
$C(Ph)HCH_2CH_3$	−2.0	−11.7	−1.5

[a] B3LYP/DZVP-LANL2DZ method.
[b] QM/MM optimisation. QM layer: B3LYP/DZVP-LANL2DZ. MM layer: UFF force field. $\alpha_{Car}=0.724$; $\alpha_{Si}=0.781$; $\alpha_N=0.700$; $\alpha_{Al}=0.793$ (default parameters in Gaussian 03).
[c] Energy single point calculation using the full QM method on the QM/MM optimised structures.

basis set [30]. This corresponds to a double-ζ basis set with polarization functions for all elements except hydrogen. For the remaining atoms in the QM part, the LANL2DZ basis set has been selected, which lacks polarization functions [31]. This basis set is called DZVP–LANL2DZ along this work. The UFF Force Field was applied for the MM subsystem [32]. The QM/MM partition layers are shown in Scheme 1.

The boundary between the QM and the MM layers was treated using a link atom to saturate the dangling atom of the QM model subsystem. The link atom used along this work was a hydrogen atom. The distance between the dangling atom and its link atom is obtained by scaling the original bond length in the 'real system' as follows

$$\alpha = \frac{l_{\text{model}}}{l_{\text{real}}} \tag{1}$$

where l_{real} is the bond length between atoms involved in the link region for the real system and l_{model} is the corresponding distance between dangling and link atoms [27]. The whole set of calculations was performed with the Gaussian03 package [33]. Convergence criteria for the geometry optimisation were: 2.5×10^{-3} hartree/bohr as the maximum element of gradient, 1.7×10^{-3} hartree/bohr as the r.m.s. of gradient element, 1.0×10^{-2} bohr as the maximum element of nuclear displacement and 6.7×10^{-3} bohr as the r.m.s. of nuclear displacement.

Transition state geometries were obtained by the STQN synchronous transit-guided quasi-Newtond method to locate an

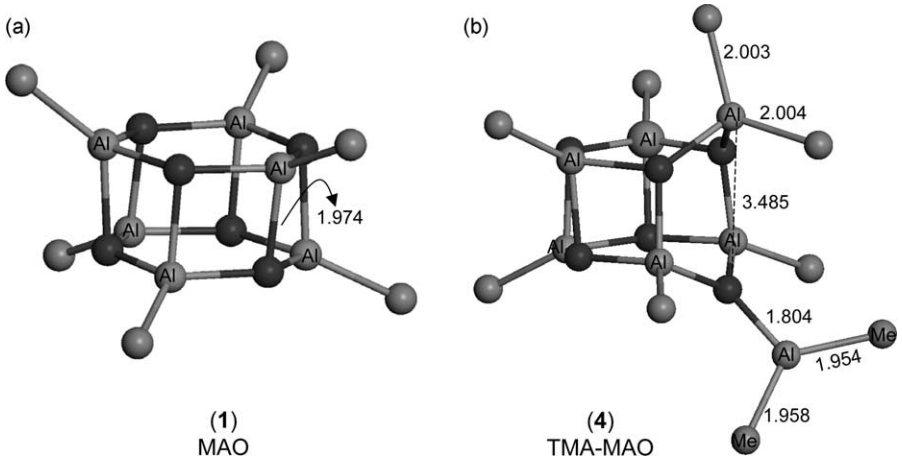

Fig. 2. Geometrical parameters for $(AlOMe)_6$ (**1**) (a) and $Al(Me)_2$–$(AOMe)_6Me$ (**4**) (b) models. Distances are given in angstrom.

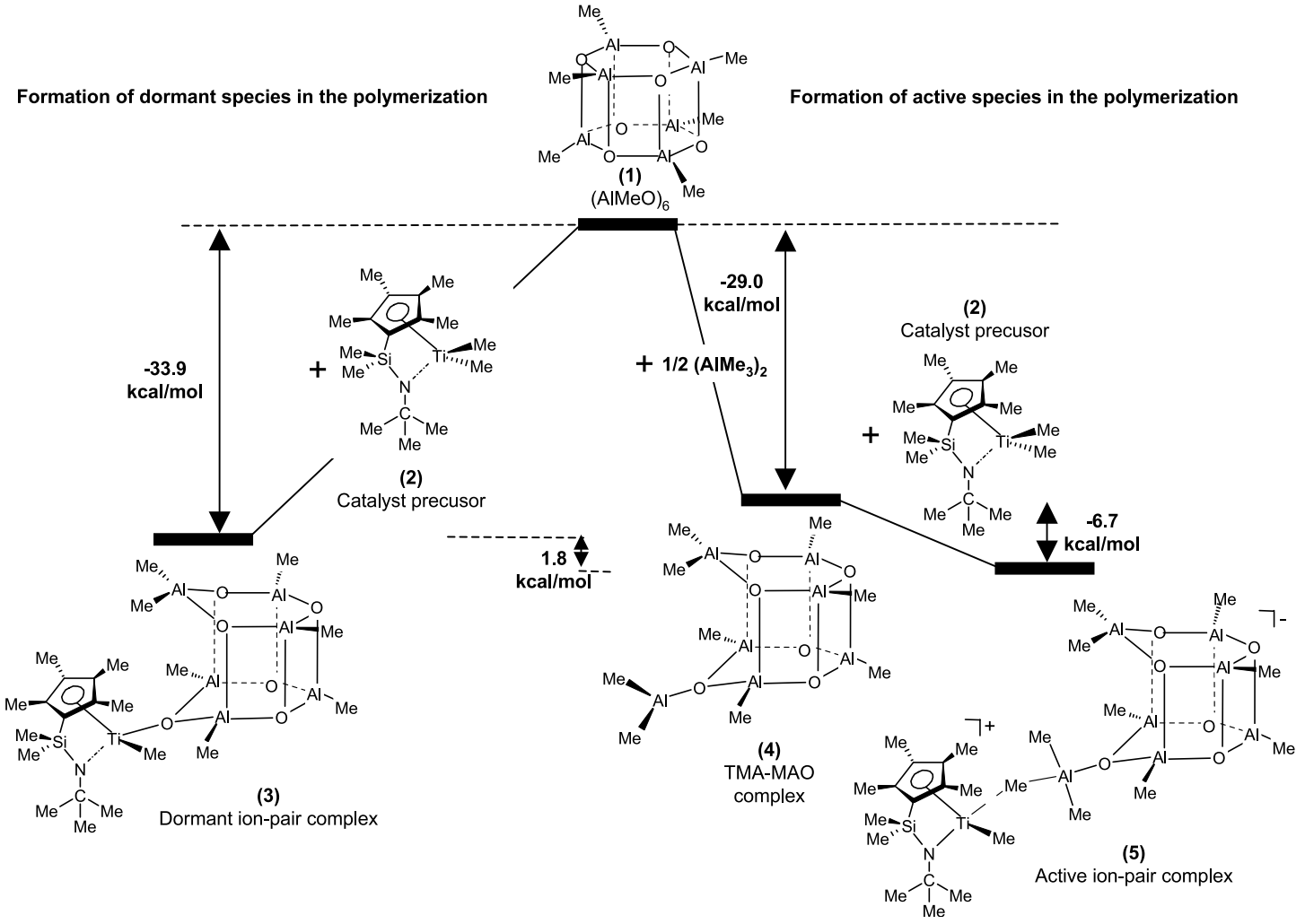

Fig. 3. Energy profiles for the formation of the dormant $[Me_2Si(C_5Me_4)(N^tBu)TiMe]^+[(AlOMe)_6Me]^-$ (**3**) and active $[Me_2Si(C_5Me_4)(N^tBu)TiMe]^+[\mu\text{-Me–Al(Me)}_2\text{–(AOMe)}_6Me]^-$ (**5**) ion-pairs. Energies are given in kcal/mol.

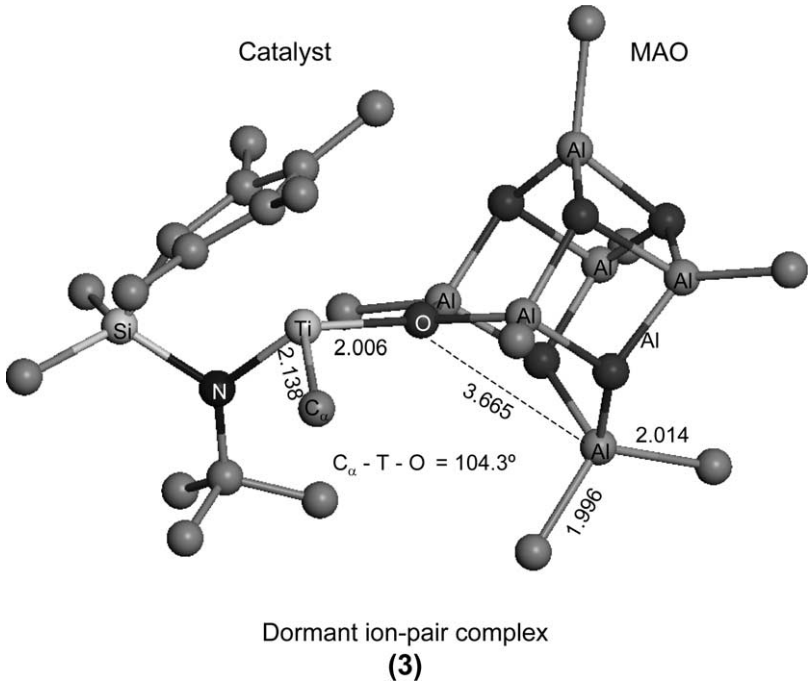

Fig. 4. Optimised structure of the dormant $[Me_2Si(C_5Me_4)(N^tBu)TiMe]^+[(AlOMe)_6Me]^-$ (**3**) ion-pair. Distances are given in angstrom.

estimated saddle-point in the path from reactant to product [34]. Subsequently, this saddle point was completely optimized following the negative eigenvector. Frequency calculations were performed to check the nature of the identified stationary points. Transition states were characterized by exactly one imaginary frequency, visualizing the corresponding eigenvector.

3. Results and discussion

First of all, the validity of the basis set and the QM/MM method used along this work is shown. Then, the formations of the active and dormant species for the ion-pair are studied. Section 3.1 is connected with the dissociation of ion-pair into the corresponding cationic and anionic species. Last of all,

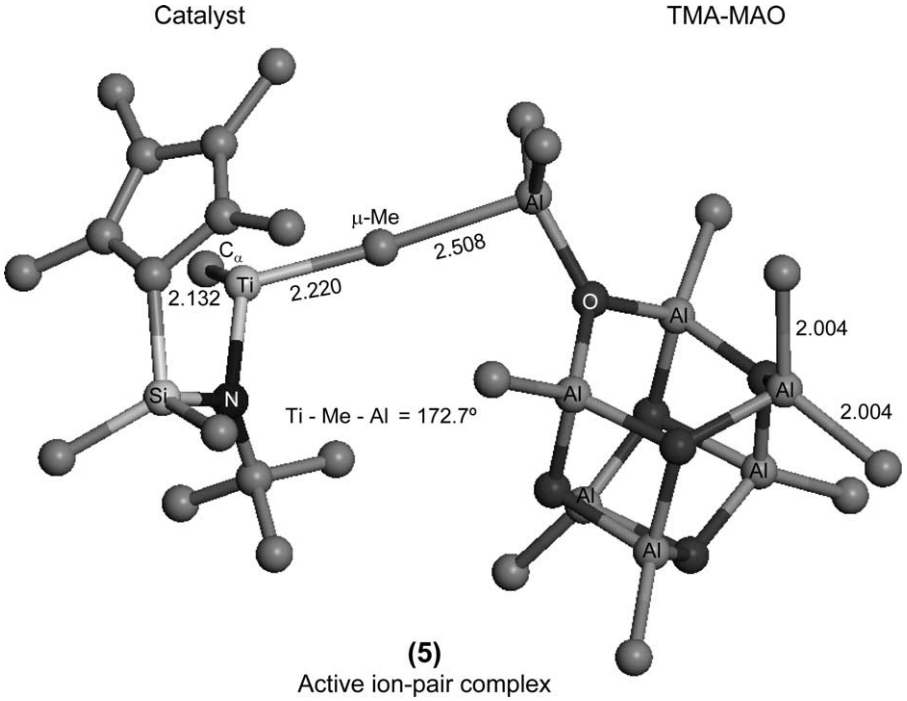

Fig. 5. Optimised structure of the active $[Me_2Si(C_5Me_4)(N^tBu)TiMe]^+[\mu\text{-}Me\text{–}Al(Me)_2\text{–}(AOMe)_6Me]^-$ (**5**) ion-pair. Distances are given in angstrom and angles in degree.

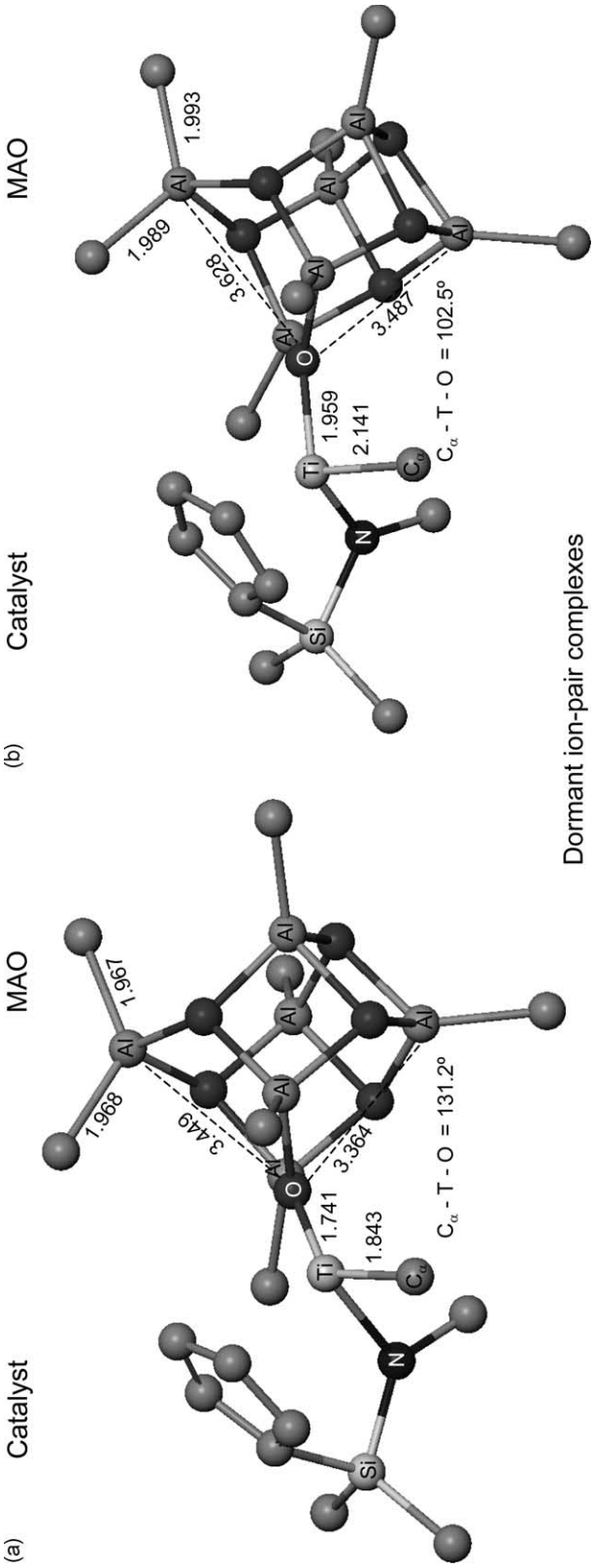

Fig. 6. Optimised structure of the dormant $[Me_2Si(Cp)(NMe)TiMe]^+[(AlOMe)_6Me]^-$ ion-pair using: (a) PWB91 pure DFT [16] and (b) B3LYP hybrid DFT with DZVP/LANL2DZ basis set.

ethylene and styrene insertion into the active ion-pair is considered.

3.1. Assessment of the DZVP–LANL2DZ basis set and QM/MM method

As it was mentioned in Section 2, a mixture of basis sets has been employed for atoms description. Specifically, DZVP basis set with polarization functions was employed for a certain set of atoms and LANL2DZ basis set without polarization functions was employed for the rest of atoms (DZVP–LANL2DZ basis set). In order to validate the application of this basis set for this system, full QM (B3LYP) calculations using a complete basis set with polarization functions for all atoms (DZVP) have been performed for $[Me_2Si(C_5Me_4)\ (N^tBu)Ti(CH_2CH_2CH_3)]^+[\mu\text{-}Me\text{–}Al(Me)_2\text{–}(AOMe)_6Me]^-$ (corresponding to the polymerisation active ion-pair species, see below Fig. 9). Evidently, calculations using the later basis set are much more computationally demanding (786 basis functions for DZVP versus 571 for DZVP/LANL2DZ). Main geometrical parameters of the ion-pair active species optimised with both basis sets are shown in Fig. 1. A similar geometry was essentially found, revealing only small differences of about 0.02 Å for distances and 3° for angles between the two basis sets.

In order to validate de QM/MM method we have performed some optimisation calculations on the active ion-pair species with different values for α factor in order to evaluate its influence on the QM/MM model. The geometry parameters for all cases are summarized in Table 1. As it can be seen, the geometries obtained with the full QM method and the different QM/MM models are quite similar. Differences smaller than 0.05 Å and 4° are found for the atoms involved in the QM/MM layer. For atoms involved in the QM layer, these differences are even smaller, except for the distance between the aluminium atom and the bridge methyl group which is about 0.1 Å larger in QM/MM models. However, we should assume this difference as unimportant due to the saving in computational resources obtained with QM/MM models. Moreover, since the geometrical parameters are not affected by the α values we have chosen the default α values given by Gaussian 03.

The formation of the following three different ion-pairs using the QM/MM model and a full QM method (see computational section for details):

$$[Me_2Si(C_5Me_4)(N^tBu)Ti(R)(Me)] + Al(Me)_2\text{–}(AlOMe)_6Me$$
$$\rightarrow [Me_2Si(C_5Me_4)(N^tBu)Ti(R)]$$
$$+ [\mu\text{–}Me\text{–}Al(Me)_2\text{–}(AlOMe)_6Me]^-$$

where R is $CH_2CH_2CH_3$, $CH_2CH(Ph)CH_3$ or $CH(Ph)CH_2CH_3$ have been studied in order to validate the chosen QM/MM. These calculations were performed with the α-parameter fixed in consideration of the above mentioned argument. These reactions correspond to the formation of the ion-pair active species after a first insertion of ethylene, 1,2-styrene and 2,1-styrene, respectively. Table 2 shows the main geometric

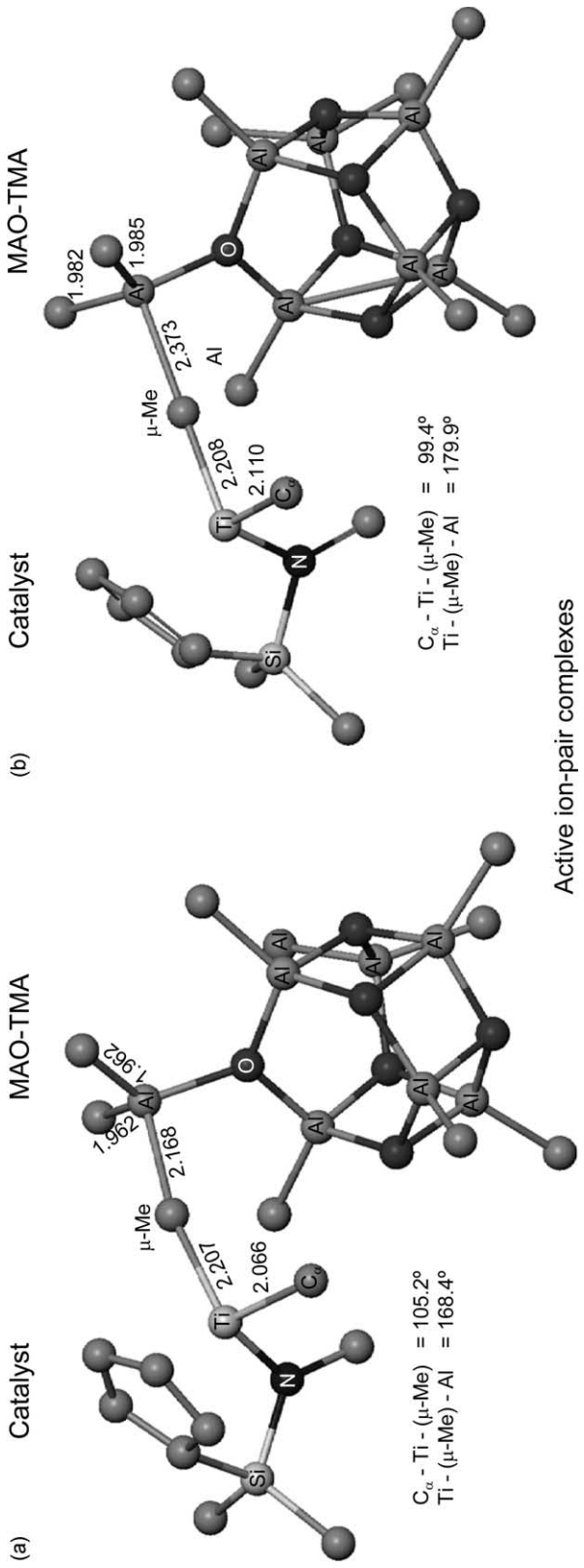

Fig. 7. Optimised structure of the active $[Me_2Si(Cp)(NMe)TiMe]^+[\mu\text{-Me–Al(Me)}_2\text{–(AOMe)}_6Me]^-$ ion-pair using: (a) PWB91 pure DFT [16] and (b) B3LYP hybrid DFT with DZVP/LANL2DZ basis set.

parameters for these complexes with both theoretical models. Comparing the distances between the full QM and the QM/MM model, it can be observed that the differences are smaller than 0.02 Å. The Ti–C(μ-Me) and Al–C(μ-Me) distances are exceptions, with differences between 0.05–0.13 Å. However, these differences are small so they can be accepted for our purposes, above all taking into account the huge decrease in the computational resources needed by the QM/MM models.

In addition, the electronic energies for the formation of each ion-pair complex are shown in Table 3. The $\Delta E_{QM/MM}$ energies are around 8–11 kcal/mol higher than the ΔE_{QM} energies. However, energy single point calculations using a full QM model on the QM/MM optimised structures (column 3 in Table 3) show differences lower than 2 kcal/mol with respect to the full QM optimised structure (column 1 in Table 3). We do not know at present the source of the differences between the energy of QM/MM and QM models, however, they are probably due to the use of UFF force field in the MM layer. Along this work, we have calculated all energies performing a single point energy calculation on the optimised QM/MM structures, which are very similar to those obtained with a full QM model as it has been demonstrated.

3.2. Formation of ion-pair complexes

The ion-pair complex is made up of the organometallic catalyst and the MAO cocatalyst species. As it was mentioned above, the cage complex $(AlOMe)_6$ has been used as a model for the MAO cocatalyst (Fig. 2a). This assumption is based on a previous theoretical study in which the most simple species containing acidic sites capable to bound TMA, thus forming species actives in the polymerisation, is the $(AlOMe)_6$ cage [9].

Experimentally, Babushkin et al. [35] proposed two different structures for the active and the dormant species in the polymerisation reaction at high MAO/catalyst ratios. The energy profile for the formation of the dormant species is sketched in Fig. 3 and the optimised structure for the dormant ion-pair complex **(3)** is shown in Fig. 4. A strong interaction between one oxygen of the MAO cage and the titanium atom ($d_{Ti–O}=2.006$ Å) can be observed. Furthermore, an Al–O bond in the squared face of the MAO has been broken as it can be deduced for the large distance of 3.665 Å comparing to the distance about 1.956–1.974 Å in the MAO molecule. The distance between the Al atom and the methyl group extracted from the catalyst is about 2.014 Å. The exothermic reaction energy for the formation of the dormant ion-pair complex (**3**) is −33.9 kcal/mol.

It has been shown that the formation of the active species in the polymerisation requires a molecule of TMA bounded to acidic oxygen in the MAO cage [15]. Thus, the formation of the active species is a two-stage reaction as is shown in Fig. 3. Firstly, the TMA species is linked to an oxygen atom in one of the hexagonal faces of the MAO, breaking an Al–O bond of the corresponding square face and transferring a methyl group to an aluminium atom in the MAO molecule (Fig. 2b). The distance between the aluminium atom and the oxygen increases from 1.974 Å in the MAO to 3.485 Å in the TMA–MAO

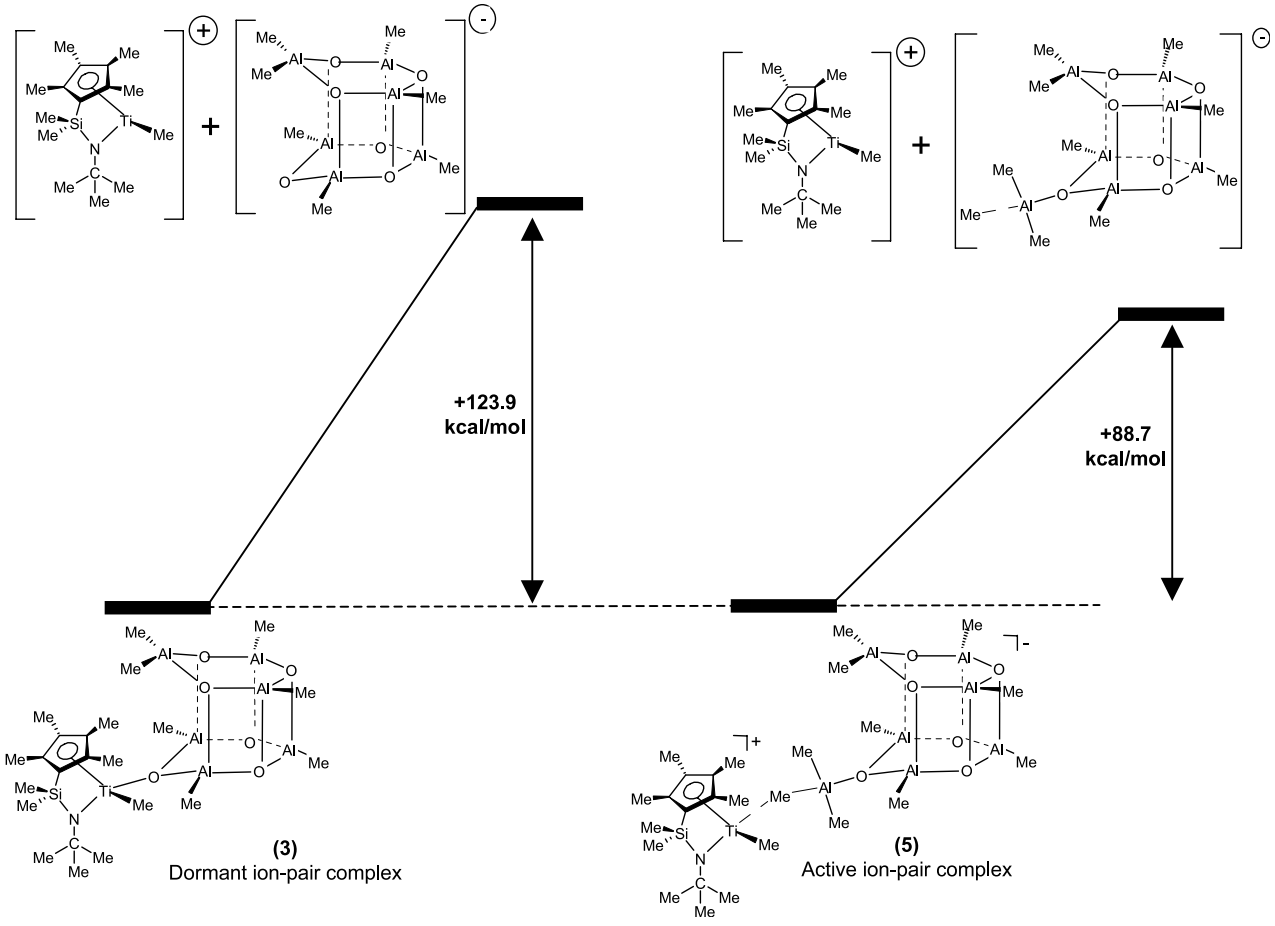

Fig. 8. Energy profiles for the dissociation of dormant $[Me_2Si(C_5Me_4)(N^tBu)TiMe]^+[(AlOMe)_6Me]^-$ (**3**) and active $[Me_2Si(C_5Me_4)(N^tBu)TiMe]^+[\mu\text{-Me–Al(Me)}_2\text{–(AOMe)}_6Me]^-$ (**5**) ion-pairs.

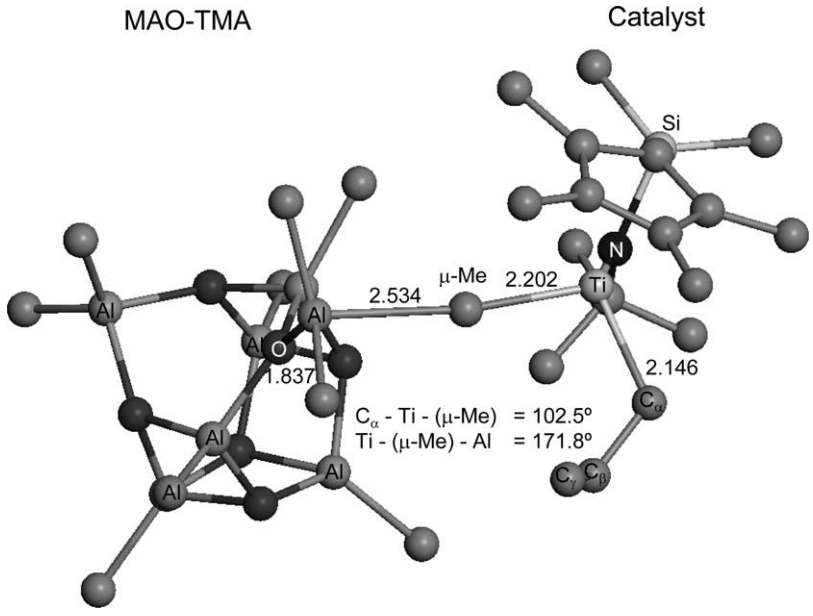

Fig. 9. Optimised structure of the active $[Me_2Si(C_5Me_4)(N^tBu)TiCH_2CH_2CH_3]^+[\mu\text{-Me–Al(Me)}_2\text{–(AOMe)}_6Me]^-$ ion-pair, resembling the active ion-pair species for the propagation mechanism. Distances are given in angstrom.

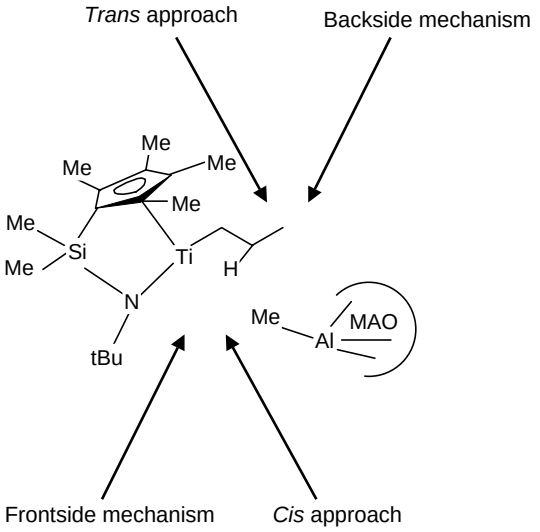

Scheme 2.

complex. At the same time, the distance of the new Al–O bond is only 1.804 Å. The coordination energy of TMA to MAO is about −29.0 kcal/mol. Secondly, the formation of the active species occurs after reaction of the TMA–MAO (**4**) compound with the catalyst precursor (**2**). The energy for this reaction is −6.7 kcal/mol. The optimised structure of the active species is shown in Fig. 5. The catalyst interacts with the TMA–MAO complex through a μ-Me bridge. This bridge is asymmetric taking into account the distances Ti–(μ-Me) (2.220 Å) and Al–(μ-Me) (2.508 Å). The Ti–(μ-Me) distance is slightly larger than the Ti-Cα distance of ca. 0.09 Å. The total energy for the formation of the active species is −35.7 kcal/mol being 1.8 kcal/mol more stable than the corresponding energy for the formation of the dormant complexes (Fig. 3).

The structures and energies for the dormant (**3**) and active species (**5**) for $Me_2Si(C_5Me_4)(N^tBu)TiMe_2$ catalyst can be compared with those found by Xu et al. [17] using a slightly different catalyst $Me_2Si(Cp)(NMe)TiMe_2$ with a pure DFT theoretical model (PWB91). They have found an energy for the formation of dormant species of −26.0 kcal/mol which is 8 kcal/mol higher than our value for the same reaction using the $(C_5(Me)_4SiMe_2N^tBu)TiMe_2$ catalyst. By comparing both structures, important differences in some geometrical parameters of about 0.25–0.30 Å between them have been noted (Figs. 4 and 6a). Some calculations using the B3LYP/LANL2DZ-DZVP method with the $Me_2Si(Cp)(NMe)TiMe_2$ catalyst have been performed in order to establish if the variations are due to the differences in the catalyst or in the theoretical model. Both structures for $Me_2Si(Cp)(NMe)TiMe_2$ are compared in Fig. 6. There are some important differences in the geometries between the calculated structures using the pure DFT model (PWB91) and the hybrid method (B3LYP). A difference of 0.25–0.35 Å is found in all the measured parameters. However, as it can be expected, the geometries of the dormant species calculated by us with the $Me_2Si(Cp)(NMe)TiMe_2$ (Fig. 6b) and the $Me_2Si(C_5Me_4)(N^tBu)TiMe_2$ (Fig. 4) catalysts are similar. Only some slight differences have been noted which can be attributed to the steric repulsion between the MAO and the C_5Me_4 (Cp*) ligand (for instance, the Ti–O distance is 0.05 Å larger in the bulkiest catalyst). Moreover, the steric interaction of the MAO with the C_5Me_4 ligand results in an orientation change of the MAO, as it can be seen comparing Figs. 4 and 6b. In addition, the structures for the $Me_2Si(Cp)(NMe)TiMe_2$ active ion-pair species calculated at B3LYP level and those reported in Xu's paper are compared in Fig. 7. The main differences between these structures are the distances involved in the Ti–Me–Al bridge. Thus, we guess that the discrepancies between our structures and energies and those calculated by Xu et al. are due to the use of a different theoretical method.

3.3. Dissociation of ion-pair complexes

Fig. 8 displays the ion-pair dissociation energies for the dormant (**3**) and active species (**5**) for the $Me_2Si(C_5Me_4)(N^tBu)TiMe_2$ catalyst. As it can be seen, the dissociation reaction is not the microscopic reverse reaction of the formation of the ion-pair. The methyl group from the precursor catalyst is completely transferred to the cocatalyst, forming one cationic species (**6**) and one anionic species (**7**) or (**8**), respectively. The ion-pair dissociation energy for the dormant species (**3**) is 35.2 kcal/mol higher than the corresponding ion-pair active species (**5**) partly due to the strong Ti–O bond in the dormant species (**3**). However, both values are very high, being a very unlike reaction at least in gas phase. It has been shown that when the solvent is taken into account this energy decreases inversely to the solvent dielectric constant increase [13]. However, the value remains too high in order to be a favourable process in the polymerisation mechanism. Consequently, the monomer insertion should occur into the active ion-pair (**5**) instead of the cationic catalyst ('naked' system). This process will be discussed in Section 3.4.

3.4. Ethylene and 1,2-styrene insertions into the ion-pair active species

In this section, the ethylene and 1,2-styrene insertions into the ion-pair active species (**9**) have been studied. The *n*-propyl group attached to the titanium atom has been used as growing chain instead of the methyl group in order to resemble the propagation step in the polymerisation reaction (Fig. 9). The Ti–(μ-Me) distance is 2.206 Å and the Al–(μ-Me) distance is 2.524 Å, being larger than the two other Al–C distances (1.975 Å and 1.974 Å, respectively). The Ti–(μ-Me) distance is larger that the Ti-Cα distances in 0.15–0.20 Å [24]. Thus, a clear (μ-Me) bridge is formed between the cationic and the anionic parts of the active ion-pair species. The distances between hydrogen in β-position on the alkyl chain and the titanium atom are rather large (3.256 and 4.103 Å, respectively), indicating that there is no evidence of β-agostic interaction between them.

The coordination of the incoming monomer in the active ion-pair species (**9**) can take place in four different ways as is sketched in Scheme 2. There are two possible orientations of the monomer with respect to the TMA–MAO cocatalyst.

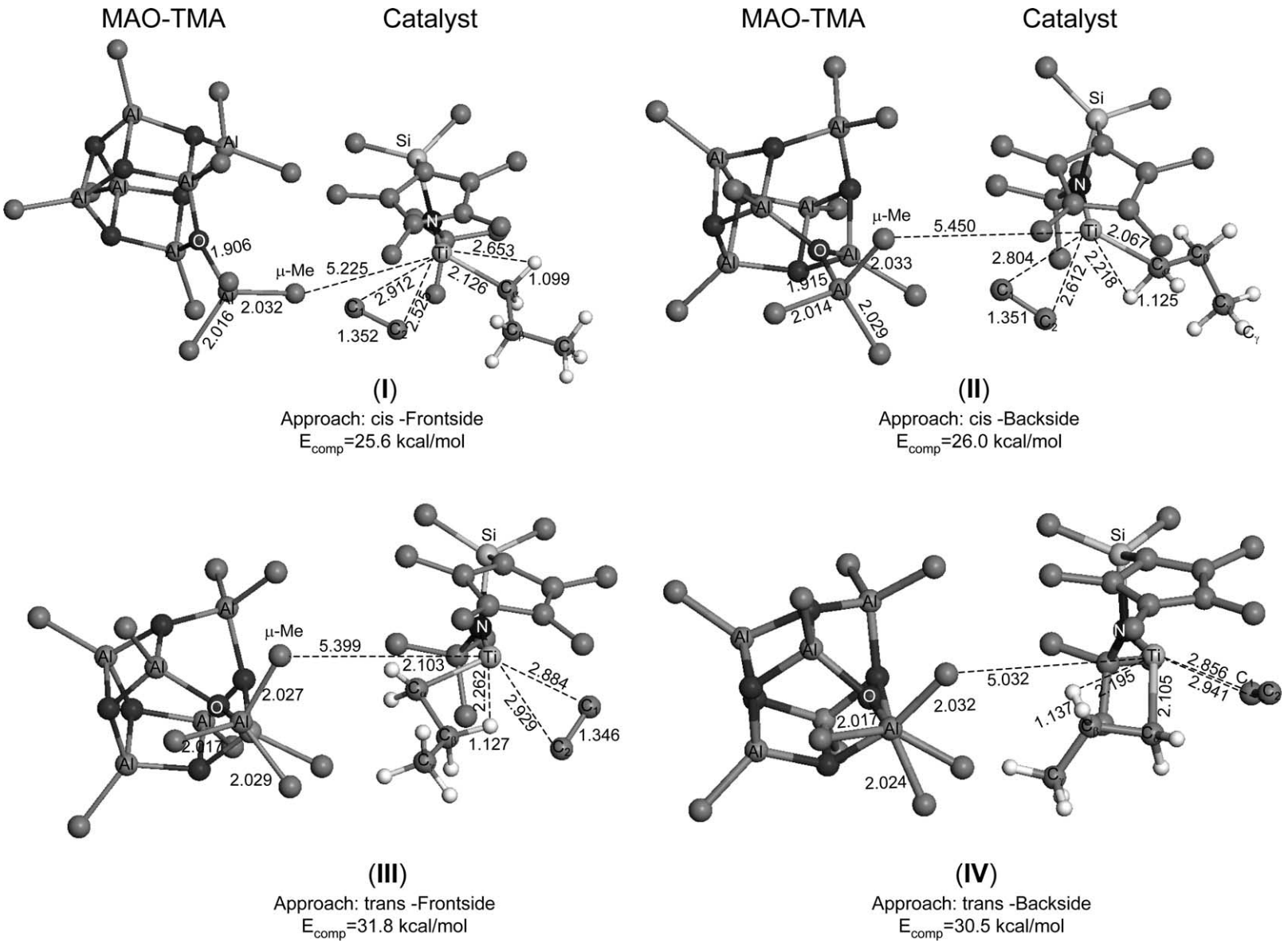

Fig. 10. Ethylene π-complexes for $[Me_2Si(C_5Me_4)(N^tBu)TiCH_2CH_2CH_3]^+[\mu\text{-Me–Al(Me)}_2\text{–(AOMe)}_6Me]^-$ ion-pair. The π-complexes energies are relative to separated species. Distances are given in angstrom.

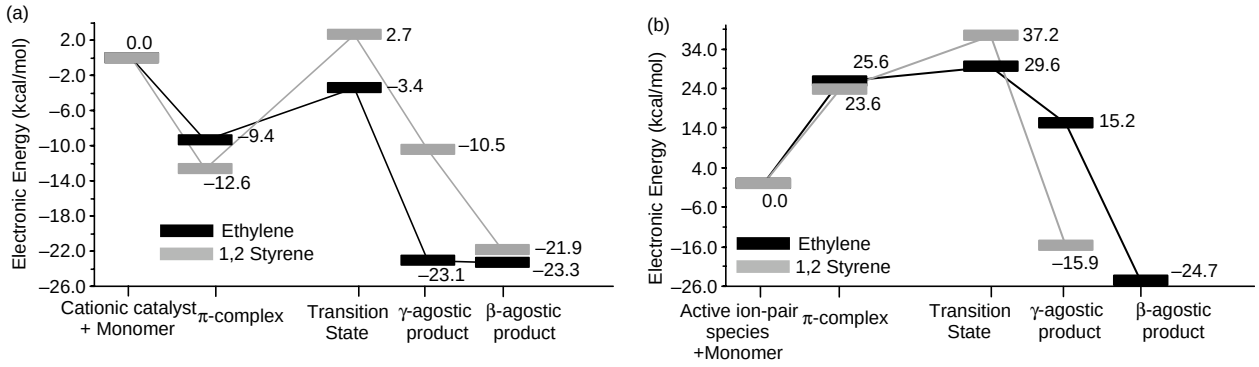

Fig. 11. Energy profiles for monomer insertion into $Me_2Si(C_5Me_4)(N^tBu)TiCH_2CH_2CH_3]^+$ 'naked' cation (a) and $[Me_2Si(C_5Me_4)(N^tBu)TiCH_2CH_2CH_3]^+[\mu\text{-}Me\text{–}Al(Me)_2\text{–}(AOMe)_6Me]^-$ (b) ion-pair. Energy values in kcal/mol are relative separated species.

The position is cis when both are in the same face and trans when they are in opposite faces. On the other hand, for each orientation there are two different ways to produce the insertion respect to the growing alkyl chain, the so-called frontside and backside insertions [21]. The four coordination possibilities have been studied for the ethylene monomer and the geometries and energies are shown in Fig. 10. It can be seen that for all π-complexes the ion-pair is partly dissociated, making room for the monomer to coordinate with the titanium atom (Ti–(μ-Me) distances larger than 5.0 Å). In all ion-pair

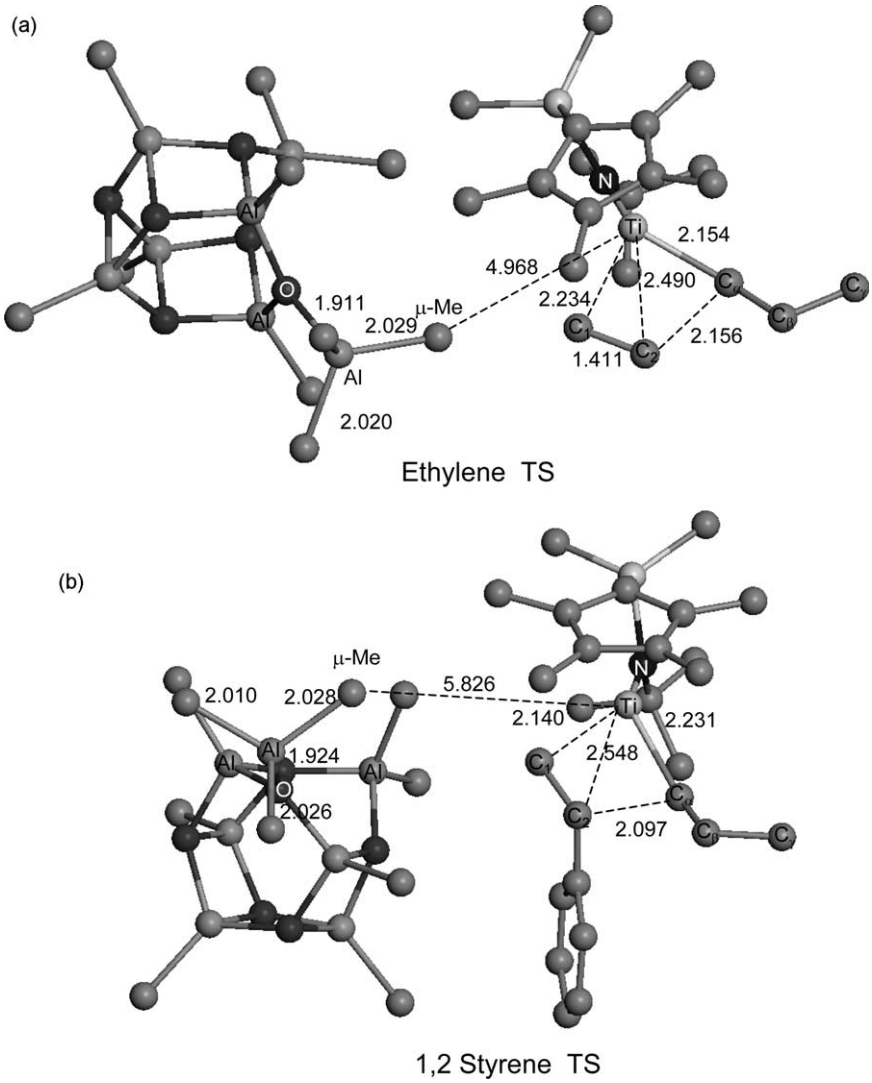

Fig. 12. Optimised structure of the transition states for monomer insertion into $[Me_2Si(C_5Me_4)(N^tBu)TiCH_2CH_2CH_3]^+[m\text{-}Me\text{–}Al(Me)_2\text{–}(AOMe)_6Me]^-$ ion-pair. Distances are given in angstrom.

π-complexes, the distances between the monomer and the metal atom are very similar to the distances in the 'naked' cationic species, which are 2.703 and 2.544 Å [25]. For the complexes **II**, **III** and **IV** the distances Ti–H_β are compatible with agostic interactions whereas this interaction is not observed in the complex **I**, as in the 'naked' cationic species case. The corresponding coordination process is endothermic with respect to the separated species with energies between 25–32 kcal/mol. This is a sharp difference with respect to the coordination step in the cationic catalyst, where this reaction is exothermic (−9.4 kcal/mol) with respect to the separated species. The most stable π-complex **I** corresponds to a cis approach of the incoming monomer and to a frontside attack of the monomer to the growing chain.

The energy profiles of the ethylene and 1,2-styrene insertions for the 'naked' and the ion-pair catalytic systems are shown in Fig. 11. As it can be seen, when the cocatalyst is taken into account the monomer coordination step is strongly endothermic: 25.6 kcal/mol for the ethylene monomer and 23.6 kcal/mol for the 1,2-styrene monomer. These coordination energies are quite high barriers for a fast polymerisation process. It has been shown that the introduction of polar solvents in the model can facilitate the partly separation of the ion-pair in the π-complex, decreasing the coordination energy of ca. 50% for the toluene solvent case [21].

Fig. 12 shows the optimised transition state structures for both ethylene and 1,2-styrene insertions. The insertion barrier is 4.0 kcal/mol for the ethylene monomer (6.0 kcal/mol for the 'naked' catalyst) and 13.6 kcal/mol for the styrene insertion (15.3 kcal/mol for the 'naked' catalyst). The relative difference between the ethylene and 1,2-styrene insertion barriers is similar in both the ion-pair (7.6 kcal/mol) and the 'naked' (9.3 kcal/mol) systems. Once the monomer is inserted the ion-pair is restored as is shown by the shorter Ti–(μ-Me) distances of about 2.200 Å found in the insertion products.

It seems that the effect of the cocatalyst is basically to raise the overall insertion barriers. It can be expected that incorporation of styrene into an ethylene/styrene copolymer would be similarly described by the ion pair as well as by the 'naked' cation.

4. Conclusions

The main goal of this paper is the theoretical study of the insertion process for the ethylene and 1,2-styrene monomers with a constrained geometry catalyst based on titanium, taking into account the presence of the cocatalyst. Due to the large size of the system a QM(B3LYP)/MM(UFF) model has been assessed and used in all calculations. The following conclusions can be drawn:

1. The smaller LANLDZ–DZVP basis set gives essentially the same geometries than that of the DZVP basis set, which is computationally much more expensive. The QM/MM model has been evaluated by comparing to full QM calculations. In general, the optimised geometries from the QM/MM method are rather similar to that found using a full QM model. Only differences of about 0.05–0.13 Å have been found for the weaker interactions in the system (bridge between methyl, TMA and titanium atoms). However, it should be accepted that these differences are small for our purposes, specially taking into account the huge saving of computational resources by using QM/MM models. Nevertheless, the energies from QM/MM calculations present some important deviations compared to full QM energies. These deviations can be diminished by performing a relatively inexpensive single point energy calculation on the optimised QM/MM structure. It is not clear where is the source of these discrepancies. It is supposed that could be related to the MM layer (UFF force field used in the calculations, the absence of electrostatic coupling between layers, etc.).
2. The formation of the active ion-pair species in the polymerisation process requires the coordination of a TMA molecule to an acidic oxygen in the MAO cage, previously to the transfer of the methyl group from the catalyst to the cocatalyst. This is a two-stage reaction with a total reaction energy of −35.7 kcal/mol. On the other hand, MAO cages without bounded TMA can generate dormant ion-pair species with a reaction energy of about −33.9 kcal/mol. So, the formation of active ion-pair species is 1.8 kcal/mol more favourable than the formation of dormant species, thus allowing the polymerisation process.
3. The dissociation processes for both active and dormant ion-pairs are very unlikely due to the high reaction energy barriers (+88.7 and +123.9 kcal/mol, respectively). Thus, the olefin insertion has to take place in the active ion-pair system instead of the 'naked' cationic catalyst.
4. The monomer coordination step into the active ion-pair species is endothermic, both for ethylene (+25.6 kcal/mol) and for 1,2-styrene (+23.6 kcal/mol). This is a sharp difference compared to similar monomer coordination into the 'naked' system which is usually exothermic. In both π-complex structures the ion-pair is partially dissociated. These energy values seem to suggest that these polymerisations should be difficult processes, although some calculations have suggested that solvent effects can reduce up to 50% these energy barriers.
5. Energy barriers for ethylene and 1,2-styrene insertion into the active ion-pair species are 29.6 and 37.2 kcal/mol, respectively. In both transition state structures the ion-pair is still dissociated. Relative differences between ethylene and 1,2-styrene insertion barriers into both the ion-pair species and the 'naked' cation have been evaluated. The similar values obtained of 7.6 kcal/mol for the ion-pair species and 9.3 kcal/mol for the 'naked' cation suggest that cocatalyst influence in monomer insertion process is quite similar for both ethylene and styrene monomers.

Acknowledgements

Thanks are due to the CICYT (Grant MAT2002-01242) for funding this investigation. S. Martínez was awarded a fellowship by the MEC. The authors also acknowledge Centro

Técnico de Informática (CTI-CSIC, Madrid, Spain), Centro de Supercomputación de Galicia (CESGA, Santiago de Compostela, Spain) and Centro de Investigaciones Energéticas, Medioambientales y Tecnológicas (CIEMAT; Madrid, Spain) for the use of their computational resources. The authors are indebted to E. Zurek for providing some structures.

References

[1] Chen YX, Stern CL, Marks TJ. J Am Chem Soc 1997;119(10):2582–3.
[2] Chien JCW, Song W, Rausch MD. J Polym Sci, Part A: Polym Chem 1994;32(12):2387–93.
[3] Zakharov II Z, Zakharov VA, Potapov AG, Zhidomirov GM. Macromol Theory Simul 1999;8(3):272–8.
[4] Zurek E, Woo TK, Firman TK, Ziegler T. Inorg Chem 2001;40(2): 361–70.
[5] Linnolahti M, Luhtanen TNP, Pakkanen TA. Chem Eur J 2004;10(23): 5977–87.
[6] Harlan CJ, Bott SG, Barron AR. J Am Chem Soc 1995;117:6465–74.
[7] Zakharov II Z, Zakharov VA. Macromol Theory Simul 2001;10(2): 108–16.
[8] Ystenes M, Eilertsen JL, Liu J, Ott M, Rytter E, Støvneng JA. J Polym Sci, Part A: Polym Chem 2000;38(17):3106–26.
[9] Zurek E, Ziegler T. Inorg Chem 2001;40(14):3279–92.
[10] Fusco R, Longo L, Masi F, Garbassi F. Macromolecules 1997;30(25): 7673–85.
[11] Fusco R, Longo L, Masi F, Garbassi F. Macromol Rapid Commun 1997; 18(5):433–41.
[12] Belelli PG, Branda MM, Castellani N. J Mol Catal A: Chem 2003; 192(1/2):9–24.
[13] Vanka K, Chan MSW, Pye CC, Ziegler T. Organometallics 2000;19(10): 1841–9.
[14] Chan MSW, Vanka K, Pye CC, Ziegler T. Organometallics 1999;18(22): 4624–36.
[15] Zurek E, Ziegler T. Organometallics 2002;21(1):83–92.
[16] Tritto I, Sacchi MC, Locatelli P, Xi Li S. Macromol Chem Phys 1996; 197(4):1537–44.
[17] Xu Z, Vanka K, Firman T, Michalak A, Zurek E, Zhu C, et al. Organometallics 2002;21(12):2444–53.
[18] Bernardi F, Bottoni A, Miscione GP. Organometallics 1998;17(1):16–24.
[19] Chan MSW, Ziegler T. Organometallics 2000;19(24):5182–9.
[20] Lanza G, Fragala IL, Marks TJ. Organometallics 2002;21(25): 5594–612.
[21] Zurek E, Ziegler T. Faraday Discuss 2003;124:93–109.
[22] Muñoz-Escalona A, Cruz V, Mena N, Martínez S, Martínez-Salazar J. Polymer 2002;43(25):7017–26.
[23] Martínez S, Cruz V, Muñoz-Escalona A, Martínez-Salazar J. Polymer 2003;44(1):295–306.
[24] Expósito MT, Martínez S, Ramos J, Cruz V, López M, Muñoz-Escalona A, et al. Polymer 2004;45(26):9029–38.
[25] Martínez S, Expósito MT, Ramos J, Cruz V, Martínez MC, Muñoz-Escalona A, et al. J Polym Sci, Part A: Polym Chem 2005;43(4): 711–35.
[26] Ramos J, Muñoz-Escalona A, Martínez S, Martínez-Salazar J, Cruz V. J Chem Phys 2005;122(7):74901–4.
[27] Maseras F, Morokuma K. J Comput Chem 1995;16(9):1170–6.
[28] Becke AD. Phys Rev A 1988;38(6):3098–100.
[29] Lee C, Yang W, Parr RG. Phys Rev B 1988;37(2):785–9.
[30] Godbout N, Salahub DR, Andzelm J, Wimmer E. Can J Chem 1992;70(2): 560–71.
[31] Hay PJ, Wadt WR. J Chem Phys 1985;82(1):299–310.
[32] Rappé AK, Casewit CJ, Colwell WA, Goddard A, Skiff WM. J Am Chem Soc 1992;114(25):10024–35.
[33] Frisch MJ, Trucks GW, Schlegel HB, Scuseria GE, Robb MA, Cheeseman JR, et al. GAUSSIAN 03 (Revision C.02). Wallingford CT: Gaussian, Inc.; 2004.
[34] Peng CY, Schlegel HB, Israel. J Chem 1993;33(4):449–54.
[35] Babushkin DE, Semikolenova NV, Zakharov VA, Talsi EP. Macromol Chem Phys 2000;201(5):558–67.